Double-layer formation in the extended Franck-Hertz experiment

Peter Nicoletopoulos*
Faculté des Sciences, Université Libre de Bruxelles, 1050 Brussels, Belgium
(Received 20 February 2008; revised manuscript received 1 June 2008; published 11 August 2008)

A model is developed which explains the collective plasma phenomena associated with the extended Franck-Hertz experiment described in an earlier paper by Nicoletopoulos [Eur. J. Phys. **23**, 533 (2002)]. The particular focus is on the formation of the free steady-state monotonic double layer. The approach used is a Bernstein-Greene-Kruskal theory in which one postulates the space potential and a suitable multicomponent electron distribution and uses Poisson's equation to solve for a physically meaningful ion distribution. A key feature is that the input space potential is chosen with a spatial scale much larger than the electron Debye length, with a restricting condition derivable from the prescribed form of *volume* production of positive ions. The model provides good quantitative agreement with the experimental results for mercury vapor, and can provide sufficient and necessary conditions for double layer formation in other atomic gases in similar experimental arrangements.

DOI: 10.1103/PhysRevE.78.026403 PACS number(s): 52.20.Fs, 52.35.Tc, 52.27.−h

I. INTRODUCTION

A. Standard versus extended Franck-Hertz experiment—from swarm to plasma

The original Franck-Hertz experiment [1] involved a "swarm" of low current electrons drifting in a gas of number density N under the influence of a uniform electric field E with an intermediate grid placed between cathode and anode designed to filter electrons with energies above a certain value. In this arrangement, spatially periodic structures develop in electron properties in a certain "window" of E/N, whose wavelength reflects the quantized nature of the atomic structure [2]. The essence of the experiment is that it produces these measurable macroscopic manifestations of fundamental, microscopic atomic properties. Although the experiment itself was first performed almost a century ago, it has only been recently that modern kinetic theoretical [2–4] and fluid modeling [5,6] techniques have been able to elucidate fully the microscopic-macroscopic connection. Otherwise this seminal experiment, which confirmed the Bohr postulates and laid the foundations of modern atomic physics, remains poorly understood and often misrepresented. The usual textbook picture for example, is effectively one of a completely unphysical "saw-tooth" periodic structure, while in reality it is smoothed due to elastic collisions [2,6]. Furthermore, the grid merely acts as a way of mirroring (not producing) the internal periodic structure in the external anode current. There is some interest in examining the way the grid operates [7], but one should never lose sight of the true essence of the experiment, which is *not* about the measurement process per se. Indeed, a less intrusive method of measurement, such as the photon flux technique reported by Fletcher [8], may be a more satisfactory option.

More recently there has been a comprehensive attempt [9–11] to elucidate the extended Franck-Hertz experiment, which is designed to show more detail than simply the recurrence of the lowest excited state. In this arrangement the electrons, rather than being subjected to a uniformly rising potential between source and grid as in the standard Franck-Hertz experiment, are accelerated in less than one excitation mean free path by an extra grid close to the cathode and allowed to travel toward a second grid across a presumed field-free region. This involves production of a *plasma* (as distinct from a swarm in the usual experiment) with associated collective phenomena, which in turn radically affect the space potential. In particular, the competition among the various species of space charge to establish overall equilibrium may lead to a pattern of *two* field-free regions separated by a narrow sheath, a steady-state *double layer*. The physics behind this experiment is yet to be fully understood, and the present paper aims at providing a theoretical model to this end.

In the standard experiment involving an electron swarm, one solves the Boltzmann equation with elastic and inelastic cross sections as input, and the field externally prescribed. The problem is linear, and one can draw upon numerical methods, which have been developed and refined over the last 30 years or so. A similar depth of understanding of the extended experiment is not possible at this time, since for plasmas one has to solve the Boltzmann equation for both ions and electrons, and couple them through Poisson's equation for the space charge field. The situation is shown in Fig. 1 of Ref. [12], and the inherent nonlinearity of the problem is evident. At some time in the future, when the necessary techniques have been developed, one should be able to make a seamless transition between swarm and plasma physics in general, and between the original and the extended Franck-Hertz experiment in particular. In the meantime, we have to improvise through the approximate and sometimes heuristic analysis, which characterizes plasma physics.

B. Extended experiment, double-layer formation, and some fundamental questions

As shown in Ref. [10], a large amount of structure in the current-voltage curve is readily displayed with the extended arrangement, but it is far from easy to find a setting of the

*pnicolet@skynet.be

 ©2008 The American Physical Society

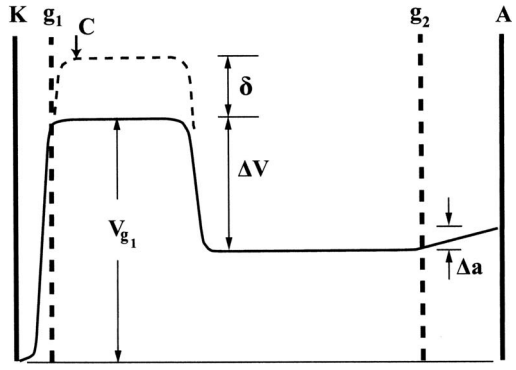

FIG. 1. Space potential between cathode (**K**) and anode (**A**) showing two field-free regions joined by a free double layer. The high-potential plasma is initially (solid curve) at the applied value of grid 1 voltage ($\mathbf{Vg}_1$), but is raised dynamically (dashed curve) by δ volts in the course of the experiment. The arrow at **C** indicates an appropriate cut used in the theory.

energy scale leading to a consistent interpretation of the excitation peaks. A picture of the space potential (drawn in idealized form in Fig. 1) was built up by analyzing the changes in the current-voltage curves under controlled variation around assumed conditions.

It was found that if a constant *decelerating* voltage (ΔV) of suitable magnitude is applied across the main collision cell (the space between the two grids), the excitation curve (namely, the plot of the current between grid $\mathbf{g}_2$ and anode **A** against the accelerating potential $\mathbf{Vg}_1$) could display *two copies* of the e^--Hg spectrum. One of them corresponds to thresholds of inelastic events excited at potential $\mathbf{Vg}_1+\delta$ and is independent of the value of ΔV. The other copy is sharper and corresponds to the same series of inelastic events incurred at potential $\mathbf{Vg}_1-\Delta V$, namely the voltage of $\mathbf{g}_2$. Increasing ΔV displaces the latter series of peaks rightwards with respect to the former. (One can thus optimize the experiment by adjusting the value of ΔV to hide the less pronounced copy.)

The obvious inferences are that

(a) The scattering cell is separated into *two* field-free, weakly ionized plasma regions, joined by a double layer (DL) whose width is no larger than one excitation mean free path.

(b) A rising wall sheath, of amplitude $\mathbf{Vg}_1+\delta$, of at most similar width, is created at the exit of the first grid culminating at the "virtual anode" **C** of the effective electron gun.

Lacking as yet is a direct confirmation that these narrow structures in the space potential are indeed present during operation; neither is it likely that a nonintrusive measurement of the potential is forthcoming in the sealed commercial apparatus used in Ref. [10]. Suggestive as it may be, the evidence presented so far to uphold the contention of DL formation remains purely circumstantial.

Obviously a more persuasive case would be at hand, if one could bring forth a physical model consistent with the main experimental observations. The first question that comes to mind is how is it possible for this potential structure to persist throughout the experiment despite the ostensible alteration of the various species of space charge as the energy of the primary beam is raised?

Two types of kinetic approach, reviewed by Raadu [13], have been developed in the literature for modeling steady-state electric double layers. One is the Bernstein-Greene-Kruskal (BGK) method, in which one starts from a prescribed form of space potential, and given phase-space distributions for all but one species of charged particles, and uses Poisson's equation to solve for a physically meaningful distribution of the remaining species. In the second method one postulates all phase-space distributions and solves for the space potential (see Sec. IX).

In discussing the BGK approach, Raadu [13] pointed out that "in principle, spatially extended quasineutral DL solutions can be found by choosing the space potential $\Phi(z)$ with a length scale much larger than the Debye length"—thus essentially eliminating the differential term in Poisson's equation. Precisely this feature is at the root of the Tonks-Langmuir model [14] for the plasma boundary, which could thus exhibit DL solutions for suitably prescribed multicomponent electron distributions. Jelić *et al.* [15] have effectively implemented this program—though not in those words—by adding a monoenergetic electron beam to the usual Maxwell-Boltzmann electron component. This theory and its bearing on the interpretation of the experimental results obtained in Ref. [10] is the main theme of the present paper.

C. Scope of the paper

We aim to develop a model which furnishes a faithful explanation of the phenomena described in Ref. [10], and which, in particular, fully supports the inferences drawn there in regard to the formation of the "free" double layer shown in Fig. 1, and is in sufficient quantitative agreement with the numerical data for mercury, to be usable for predicting whether DL formation should or should not occur in other atomic gases, in similar experimental arrangements, under a predeterminable set of conditions.

The theory itself is particularly attractive because the space potential initially input in the BGK method is not obtained merely by an educated guess: A one-parameter class of potentials—containing the final answer—is derivable analytically at the outset by way of the Tonks-Langmuir prescription of volume ionization, which acts like a closure condition. The authors of Ref. [15] noted the existence of double-layer solutions, but doubted both their mathematical consistency and their physical meaning. These doubts will be dismissed here: It will be shown that the DL or "DL-like" structures of Ref. [15] are *bona fide* double layers in all respects. The paper is organized as follows: Sec. II A gives a summary of the experimental facts presented in Ref. [10], with supplemental information, obtainable quantitatively and visually, on the evolution of the discharge toward the stable form governed by the space potential shown in Fig. 1. This summary clarifies the physical objectives of the model, and sets the goals of the theory, as outlined in Sec. II B. Readers interested only in a theory of DL formation may skip Sec. II and proceed directly to Sec. III. Onwards from Sec. III, in the interest of simplicity, the physical arguments and the subsequent theory are presented in parallel plane geometry. (In the actual apparatus only the first grid is planar; the other

three electrodes are concentric cylinders.) Sections III–V are devoted to elaborating the basic theory and obtaining the DL solutions. In Sec. VI the model is refined in regard to certain idealized features (such as the assumption of a cold electron beam) and, in Sec. VII, it is extended, by including a monoenergetic ion beam—an important element in the experiment of Ref. [10]. Section VIII is a detailed comparison of the theoretical results with the experimental facts listed in Sec. II. Section IX is an appraisal of the model in connection to related literature. Section X contains some comments on the basic physical assumption of free-fall motion. A summary with conclusions is given in Sec. XI.

II. REVIEW OF MAIN EXPERIMENTAL OBSERVATIONS

A. Evolution of the discharge

The experiment is carried out on mercury at vapor pressures of 3–5 Torr. The distance between the grids $\mathbf{g}_1$ and $\mathbf{g}_2$ is about 1 cm. The potential configuration shown in Fig. 1 sets in abruptly in two steps, at critical values called $\mathbf{C}_1$ and $\mathbf{C}_2$ of the accelerating potential $\mathbf{Vg}_1$.

It is possible to ascertain highlights in the evolution of the discharge, and to quantify the voltages $\mathbf{C}_1$ and $\mathbf{C}_2$, by peering through the top end of the cylindrical structure while tracing curves of the type shown in Ref. [10]. As the voltage $\mathbf{Vg}_1$ is raised, the visible part of the region between the electrodes appears at first dark. When $\mathbf{Vg}_1$ reaches the lowest excited state (^3P) of mercury (see Figs. 2–6 in Ref. [10]) two localized blue-green glows are born, seemingly bordering the flat sides of the first grid, and stretching in opposite directions towards the second grid as the voltage increases.

The positive ion current at the anode can be monitored separately by a small modification in the grid-anode circuit. Curves recorded with that arrangement show that a weak ion current sets forth concurrently with the glows. Although a small amount of ions are being produced within the glows [by cumulative ionization via the metastable (6^3P_0 and 6^3P_2) members of the triplet of lowest excited states], swarm conditions are still prevailing and the current-voltage curve is essentially drawing the first peak of the *standard* Franck-Hertz experiment.

In different samples of the tube the rates of elongation of the glowing paths in each direction may differ. When the outer edge of a glow reaches $\mathbf{g}_2$, the entire half-volume on that side is lit up and the color changes to pinkish. This transition occurs precisely at the point where the voltage at $\mathbf{g}_2$ reaches 4.7 V, the threshold of the lowest excited state (6^3P_0). Therefore $\mathbf{C}_1=\Delta V+4.7$ V.

Past the point $\mathbf{C}_1$, volume generation of positive ions evidently extends all the way to the grid $\mathbf{g}_2$. Peaks in the current-voltage curve corresponding to the next higher thresholds ($6^3P_1, 6^3P_2, 6^1P_1, \ldots$) excited by the primary beam at the *lower potential*, may or not emerge from then on, showing that a sufficient extent of field-free drift space adjacent to $\mathbf{g}_2$ may or may not have been generated, and hence the "free" double layer shown in Fig. 1 may or may not have developed.

The ion current increases substantially at $\mathbf{C}_1$, but the ring of gas between $\mathbf{g}_2$ and the anode remains dark. The absence of visible light in that zone persists throughout the experiment, indicating that plasma conditions never extend beyond grid $\mathbf{g}_2$: The zone of gas between the grid and the anode is governed by swarm physics; such circumstances are a basic requirement for ensuring the type of microscopic kinetics responsible for displaying the low-potential spectrum in the electron current between grid $\mathbf{g}_2$ and the anode $\mathbf{A}$, as explained in Ref. [11].

A short further increase of $\mathbf{Vg}_1$ is followed by a sharp kink in the excitation curve (marked as feature $\boldsymbol{A}$ in Figs. 2–6 of Ref. [10]). This is the second critical voltage, $\mathbf{C}_2$. The value of $\mathbf{C}_2$ ($\cong$9.5 V) is close to the ionization threshold of mercury (10.4 eV) and indeed the level of ion current rises abruptly at the kink by at least an order of magnitude. So strong is this ion current sometimes, that a positive potential must be applied between $\mathbf{g}_2$ and the anode ($\Delta\mathbf{a}$ in Fig. 1) to prevent the excitation curves from dropping below the zero axis. It is noteworthy that this current cancellation phenomenon occurs only at the larger settings of ΔV.

The onset of beam-excited single-stage ionization near $\mathbf{g}_1$ produces a sudden shift in the high-potential energy scale: Subsequent peaks in the high-potential copy of the spectrum correspond to excitations at voltage $\mathbf{Vg}_1+\delta$ rather than $\mathbf{Vg}_1$. Both the magnitude of δ and the position of $\mathbf{C}_2$ (feature $\boldsymbol{A}$) depend on the pressure of mercury gas and on the strength of the cathode emission current, but are independent of ΔV. At optimal discharge conditions the values of these voltages are consistently found to be $\delta=2.6\pm0.1$ and $\mathbf{C}_2=9.5\pm0.1$.

Apart from producing a shift in the high-potential voltage scale, the changes occurring in the discharge at $\mathbf{C}_2$ do not affect the high-potential copy of the spectrum. The changes do affect, however, some of the low-potential peaks: any of the latter class that have been shifted *beyond* feature $\boldsymbol{A}$ (by increasing ΔV), are much stronger than they would otherwise be (at lower ΔV). Ostensibly, a more substantial width of field-free plasma at the potential of $\mathbf{g}_2$ is present beyond $\mathbf{C}_2$ from then on.

It should be stressed however, that the creation of the low-potential copy of the spectrum is by no means guaranteed. Its emergence and continued presence is contingent on the following two conditions:

(1) The current emitted by the oxide-coated cathode must be adequately strong. Furthermore, the initial beam must be sufficiently cold.

Therefore the state of activation of the oxide-coated cathode is a crucial factor: raising the current by overheating a poorly activated (high work function) cathode widens the energy distribution of the primary beam and will not do (see Ref. [10], Sec. 8.)

(2) The total potential difference $\Psi=\Delta V+\delta$ must be sufficiently large.

In actual fact there are both lower and upper bounds, namely, $4.7<\Psi<7.6$ (in volts). Below $\Psi=4.7$ only high-potential peaks are seen, regardless of primary beam conditions. Past 4.7 V, both classes of peaks (say high and low features) are present, and the strength of the low class increases with the setting of Ψ and attains a maximum at $\Psi\approx6.7$. At this point the high peaks are masked and never reappear. Past $\Psi=6.7$ the peaks decline in strength and eventually disappear amidst a noisy signal. Presumably, the "free"

double layer is closer to the first grid at the better settings of Ψ, so that a larger proportion of field-free space exists at the lower potential. What is interesting is that the optimal interval $4.7<\Psi<6.7$ corresponds exactly to the range of fine splitting of the $6P$ state, the lowest excited state, whose members $(6^3P_0, 6^3P_1, 6^3P_2, 6^1P_1)$ have by far the largest inelastic electron-scattering cross sections.

B. Goals of the theory

The aim now is to construct a steady-state model applicable to the final stage of the discharge. Primarily, the theory should be capable of showing *unequal* widths of low- and high-potential plasma on each side of a double layer, and should thus reveal the mechanism leading to the two extreme configurations where one or the other of the two plasmas invades the entire intergrid region. In particular, the model should elucidate the basic factors of large enough decelerating intergrid potential, and sufficiently strong and cold primary electron beam, and should thus clarify their role in the formation of the low-potential plasma.

Also explainable should be the apparent sudden displacement of the DL further leftwards toward the first grid, at the threshold of beam-excited single-stage ionization, as described above in Sec. II A.

Finally, the theory should be capable of showing the observed near-cancellation of the total current, upon DL formation, at the larger settings of Ψ. The ratio of electron and ion currents—called the Langmuir ratio—is an important parameter in electric double-layer physics. In most cases [13] this ratio is very large, of the order of $(M/m)^{1/2}$, where M and m are the atomic and electron masses. For mercury, $(M/m)^{1/2}=607$. Evidently, in the experiment of Ref. [10] the Langmuir ratio can be as much as 607-fold smaller than usual, and a theoretical model has no real chance of being successful unless it can explain this.

The upward shift (δ) of the space potential in close vicinity of the first grid has been described before [16,17], in similar experiments with various gases, each gas producing a different stable value of δ, but a good theoretical description of this phenomenon is still at issue. The fast transitions at $\mathbf{C}_1$ and $\mathbf{C}_2$ require a time-dependent approach and should also be studied in their own right in the future.

III. PHYSICAL SYSTEM

The part of the discharge to be modeled occupies the space between a small extent of plasma, acting as a virtual anode, and a plane close to the second grid. Within this region the potential Φ is decreasing monotonically from zero to the imposed value $-|\Psi|$ with $|\Psi|=\delta+\Delta V$ V. Specifically, the left boundary $\Phi=0$ of our model is taken to be at the point $\mathbf{C}$ in Fig. 1, near the edge of the accelerating sheath, which has climbed above the applied value $\mathbf{V}_{\mathbf{g}_1}$ past the grid $\mathbf{g}_1$, culminating at potential $\mathbf{V}_{\mathbf{g}_1}+\delta$.

In the first stage of the theory, the electron velocity distribution is assumed to be a superposition of two components: A Maxwell-Boltzmann group (temperature T, density n_0 at $\Phi=0$), and a delta function $\sim\delta[mV^2-2e(|\Psi|+|\Gamma|+\Phi)]$ corresponding either to a single monoenergetic beam of unspecified direction, or to identical oppositely streaming beams (total density n_b at $\Phi=0$, kinetic energy $mV^2/2=e|\Gamma|$ at $\Phi=-|\Psi|$; e,m,V, being the electron charge, mass, and velocity). Streaming beams arise from inelastic scattering of the primary beam in the high-potential field-free region. Counterstreaming beams are produced by similar events in a small zone between the plane at $\Phi=-|\Psi|$ and $\mathbf{g}_2$ which acts like a virtual cathode. Integrating the electron distributions over velocity gives the total electron density: $n_e(\Phi)=n_0\exp(e\Phi/kT)+n_b[1+\Phi/(|\Psi|+|\Gamma|)]^{-1/2}$ (where k is Boltzmann's constant).

Ions are created at a constant rate ν throughout the volume of the discharge, in a manner to be prescribed. Between the grids, electron and ion motion is determined only by the self-consistent electric field (readers who feel uncomfortable with this assumption could glance at Sec. X).

In a later stage of the theory, an additional positive component, a cold ion beam, will be added to the ion velocity distribution. The ion beam is prepared by single-stage ionization in the region between the cathode K and the point $\mathbf{C}$. It is then injected into the volume of the discharge, at $\Phi=0$, with initial energy $|\Theta|$ and density p_b and contributes an additional term $p_b[1-\Phi/|\Theta|]^{-1/2}$ to the ion density.

IV. THEORY

Following Tonks and Langmuir [14], let us assume that positive ions of mass M and charge e are generated *at rest* at any position z past the point $z=0$ at $\Phi=0$, and *free fall* towards $\mathbf{g}_2$ $(z=z_G)$ in the negative monotonic self-consistent potential. An ion formed at $z_1<z$ has a velocity at z of $U_z=(2e/M)^{1/2}(\Phi_1-\Phi_z)^{1/2}$, where Φ_1 is the potential at $z=z_1$. Assuming also that the ions are generated at a constant rate ν, the ion density $n_i(z)$ at z is

$$n_i(z)=\int_0^z \frac{\nu}{\sqrt{(2e/M)(\Phi_1-\Phi_z)}}dz_1. \tag{1}$$

If $G(U,z)dU$ is the number of ions at z having velocity in the range U to $U+dU$ it follows that $G(U,z)dU=\nu\,dz/U$. In a collisionless regime, the ion total energy $X=e\Phi+MU^2/2$ is a constant of the motion. Hence, in $[U,e\Phi(z)]$ phase-space coordinates, the ion distribution depends only on the total ion energy X and it turns out that

$$G(X)=-\frac{M}{e}\nu\frac{dz}{dX}, \tag{2}$$

where X varies from $e\Phi$ to zero. The derivation of Eq. (2) has been carried out in Ref. [18] by adding a source term $\sim\nu\delta(U)$, describing ion gain, to Vlasov's kinetic equation for the ion distribution function, where $\delta(U)$ is a Dirac function signifying that ions created by ionization have vanishing initial velocity.

Converting to dimensionless quantities, Eq. (2) takes the form $F(x)=ds/dx$, and Poisson's equation $d^2\Phi/dz^2=(-e/\epsilon_0)(n_i-n_e)$ is given by

$$\alpha^2 \frac{d^2\phi}{ds^2} = \int_0^\phi \frac{F(x)}{\sqrt{2(\phi - x)}} dx - e^{-\phi} - \frac{N}{\sqrt{1 - \phi/(\psi + \gamma)}}, \quad (3)$$

in which $x=\phi-u^2/2$, and the dimensionless quantities are $F(x)=(kT/M)^{-1/2}G(X)$, $x=-X/kT$, $\phi=-e\Phi/kT$, $\psi=e|\Psi|/kT$, $\gamma=e|\Gamma|/kT$, $u=U(kT/M)^{-1/2}$, $N=n_b/n_0$, $s=z/L$, $\alpha=\lambda/L$, $L=(kT/M)^{1/2}/\nu$, and $\lambda=[\epsilon_0 kT/e^2 n_0]^{1/2}$.

For mercury, the length scales L and λ in cm, with density in cm^{-3}, and $kT=\tau$ in eV, are given by $L=6.9\times10^4(\tau^{1/2}/\nu)$ and $\lambda=743[\tau/n_0]^{1/2}$, and therefore $\alpha=0.011\nu n_0^{-1/2}$. The parameter α determines the degree of charge neutrality in the plasma.

Solutions of Eq. (3) are sought by the following procedure. We assume that α is very small and begin by seeking the solution $F_0(x,N)$ of the resulting integral equation in the "plasma approximation" $\alpha=0$. In the present case, this solution can be obtained semianalytically by Abel inversion [19]. For given values of ψ and γ, a range $N>N_0$ of the density ratio N is determined in which the solution $F_0(x,\phi;N)$ is physically meaningful. Equation (2) leads to

$$s(\phi,N) = \int_0^\phi F_0(x;N)dx. \quad (4)$$

Equation (4) and the inverse relationship $ds/d\phi=F_0(\phi;N)$ are the cardinal features of the Tonks-Langmuir model.

From Eq. (4), the corresponding family of space potentials $\phi(s,N;N>N_0)$ can be obtained implicitly. For N near the lower boundary N_0, and small γ, it will turn out that these solutions exhibit a narrow sheath followed by a considerable extent of low-potential plasma.

In order to proceed to the general case where $\alpha\neq0$, the differential term $\alpha^2(d^2\phi/ds^2))$ in Poisson's equation must be expressed as a function of ϕ, using the inverse function $s(\phi)$. This is given by $\Delta n(\phi)=\alpha^2(d^2s/d\phi^2)(ds/d\phi)^{-3}=\alpha^2[dF_0(\phi)/d\phi][F_0(\phi)]^{-3}$. The modified form $F_\alpha(x,N)=F_0(x,N)+\Delta F_0(x,N)$ of the ion phase-space distribution at $\alpha\neq0$ can now be found by numerical Abel inversion of $\Delta n(\phi)$. A range $N>N_\alpha>N_0$ generally exists in which the new distribution $F_\alpha(x,N)$ is physically meaningful. The subset $\phi(s,N;N>N_\alpha)$ of the previously obtained family of solutions is the final answer. It will be seen below that, for small α and values of N close to the new lower bound N_α, the DL is still very narrow.

At this point the BGK scheme for finding a DL solution has been fully implemented: starting from a two-component electron distribution and a DL-like form of the space potential, namely, $\phi(s,N;N>N_0)$, an ion energy distribution $F_\alpha(x,N;N>N_\alpha)$ has been computed that is physically reasonable, i.e., positive and with no singularities everywhere in phase space. The spatial scale of $\phi(s)$—essentially the ionization mean free path—is determined from the values of M, ν, and T in the discharge, and thanks to the assumed form of internal volume ionization, which implies Eq. (4) and the inverse relationship $F_0(\phi)=ds/d\phi$, no element of guessing is involved in prescribing the input space potential.

It should be clear, however, that from the point of view of the BGK method, Eqs. (2) and (4) are irrelevant. One could conceivably have guessed the above expression $\phi(s,N)$ for the space potential, and then used Eq. (3) to calculate the missing ion distribution and to show that it has no unphysical features—provided that N is large enough. He would end up with the same result. Nevertheless, he would be at a loss to explain the physical basis of his guess.

Lest the reader be surprised by the fact that the space potential is directly calculable from Eq. (4), it is helpful to translate the picture to more conventional DL language. Monotonic collisionless double layers are solutions of Poisson's equation $d^2\phi/ds^2=n(\phi)$, where $n(\phi)$ is the total charged particle density, with the boundary conditions (I) $n(\phi)=n(\psi)=0$ (charge neutrality) and (II) $d\phi/ds=0$ at $\phi=0$ and $\phi=\psi$ (zero electric field). A first integration from zero to ϕ yields $(1/2)(d\phi/ds)^2+V(\phi)=0$, where $V(0)=0$; the function $V(\phi)$ is the "Sagdeev potential" [13] (the negative of the normalized Maxwell stress). The boundary conditions (I) and (II) imply that $V(\phi)$ is an inverted bell-shaped curve between $\phi=0$ and $\phi=\psi$. In addition, self-consistency between the electric field and charges near the boundaries require that, for a monotonic potential, the net charges on the low- and high-potential side are negative and positive, respectively. This implies another existence condition, namely, that (III) $V''(\phi)<0$ at both end points, which is the generalized Bohm criterion for a double sheath [13], and ensures that the DL is shielded from the ambient plasmas.

Given $V(\phi)$, the space potential $\phi(s)$ is calculable implicitly by simple quadrature and will obviously be of the steplike form shown in Fig. 1. In the present case, $n(\phi)=\Delta n(\phi)/\alpha^2$ and therefore

$$V(\phi) = -(\alpha^2/2)[F_0(\phi,N)]^{-2}. \quad (5)$$

Of course, here there is no need to perform the integration because the solution $\phi(s,N;N>N_1)$, alias "BGK equilibrium," is already known, and conditions (I)–(III) have been satisfied automatically, as can be verified explicitly (see below) by using Eq. (5) to calculate $V(\phi)$. As pointed out in Ref. [13], the interesting conclusion is that in the BGK approach, the boundary conditions are met simply by prescribing that the ion phase-space distribution should be positive.

The condition $V(0)=V(\psi)=0$ is a requirement of stress balance: the total particle pressures, dynamical and "thermal," must be in balance across the double layer. This is the generalized Langmuir condition [13]. The case mentioned in Sec. II B, where the "Langmuir ratio"—conventionally given by $\Lambda=(m/M)^{1/2}(I_e/I_i)$, where I_e and I_i are the ion and electron current densities—is close to unity, requires that the dynamical pressures of externally injected particle beams dominate. In the present case any ions emerging at $\phi=\psi$ have been created internally, and one can no longer expect that $\Lambda\cong1$ at both ends of the discharge region. The extreme case of current cancellation implied by the data of Ref. [10] would imply that, at $\phi=\psi$, $\Lambda=(m/M)^{1/2}$.

The ion flux density at $\phi=\psi$ is obtainable by integrating the quantity $uF[x(u)]$ over u, and is thus given simply by $n_0(\tau/M)^{1/2}s(\psi)$. Hence, for a single beam of either direction

$$\Lambda(\psi) = [j(\psi) + N[(2\psi + 2\gamma)^{1/2}]/s(\psi) \ , \quad (6)$$

in which the quantity $n_0(\tau/m)^{1/2}j(\psi)$ is the random electron flux density at $\phi=\psi$. We are now ready to apply the theory to the mercury discharge of Ref. [10].

V. RESULTS

Before proceeding to the solutions, we need a reasonable estimate for α, the charge-neutrality parameter (a more appropriate name would be "Tonks-Langmuir number" in analogy to the "Reynolds number" in fluid physics, that similarly controls the weight of a differential term).

The present type of 1-cm-wide discharge, between concentric cylinders, at a few Torr, is parallel in most respects to the "anchored ball of fire" mode of thermionic discharge, discussed extensively by Johnson [16] for rare gases. Typical values of temperature τ and bulk density n_0 found in Ref. [16] for the heavier element (Xe) are around 1 eV and 10^{13} cm^{-3}. It will seen in the next section that with $\tau \cong 1$ eV, and values of potential $|\Psi|$ characteristic to the experiment of Ref. [10] with mercury, the *computed* value of the dimensionless distance $s(\psi)$ is close to 1. Hence the spatial scale is $L \cong 1$ cm. This implies that $\nu \cong 6.9 \times 10^4$ s^{-1}.

Another set of experimental data [20], this time on positive columns of mercury discharges of transverse radius R, shows that at low gas pressure p the combined quantity $R\nu(Rp)$ is a descending function of Rp. At $Rp=0.1$ Torr cm this function levels off, so that at higher pressures $R\nu(Rp) \cong$ const and $\nu \cong 7 \times 10^4$ s^{-1} (the figure found above) regardless of radius; the corresponding electron temperature (as computed in Ref. [20], using the "plasma balance" equation of Ref. [14]) is, once more, $\tau \cong 1$ eV.

Therefore it may not be far amiss to assume that, at operating pressures of a few Torr, the choice $L \cong 1$ cm, $\lambda/L = \alpha = 0.011 \nu n_0^{-1/2} \cong 2.35 \times 10^{-4}$ represents fairly closely the experimental conditions of Ref. [10].

To facilitate the actual comparison to experiment, we replace dimensionless energy variables (ϵ) by products ($\beta\epsilon$) of dimensional quantities. Hence the term $\exp(-\phi)$ in Eq. (3) is changed to $\exp(-\beta\phi)$, so that potentials are expressed directly in volts and the electron temperature is β^{-1} eV. As stated in Sec. IV, the solution of the "plasma equation" ($\alpha = 0$) is obtainable semianalytically by Abel inversion [19], yielding.

$$F_0(x) = \frac{\sqrt{2}}{\pi}\left\{\frac{1}{\sqrt{\beta x}}\left[1 + \frac{N(\psi+\gamma)}{\psi+\gamma-x}\right] - \sqrt{\pi}e^{-\beta x}\,\mathrm{erfi}(\sqrt{\beta x})\right\}, \tag{7}$$

where $\mathrm{erfi}(y)$ denotes the error function of imaginary argument [$\mathrm{erfi}(y)$ is $2\pi^{-1/2}$ times the Dawson integral $D(y) = \int_0^y \exp(w^2)dw$]. From Eqs. (4) and (7), the space potential $\phi(s)$ between 0 and ψ is given implicitly by

$$s(\phi) = \frac{\sqrt{2}}{\pi}\left\{2N\sqrt{\beta(\psi+\gamma)}\,\mathrm{arctanh}\left[\frac{\sqrt{\phi}}{\sqrt{\psi+\gamma}}\right] + \sqrt{\pi}e^{-\beta\phi}\,\mathrm{erfi}(\sqrt{\beta\phi})\right\}. \tag{8}$$

Figure 2 shows the ion energy distribution $F_0(x)$ obtained from Eq. (7) with $\beta\psi=3$, $\beta=1$, $N=0.15$, for various values of the "energy excess" at $\phi=\psi$, represented by the quantity $\beta\gamma$. In each case the function $F_0(x, N=0.15)$ has a deep minimum where $F_0 \cong 0$. Given that $F_0(x) = dx/d\phi$, this means that a narrow layer (a "free" sheath in conventional parlance) is being formed within the volume between 0 and ψ. The part of $F_0(x)$ due to the bulk electron density is known as the Harrison-Thomson distribution [21], which becomes negative at $x=0.854$. The additional density due to the electron beam renders $F_0(x,N)$ physically meaningful, i.e., positive and nonsingular, throughout the range of energy x in the discharge. This imposes a lower bound on the parameter N.

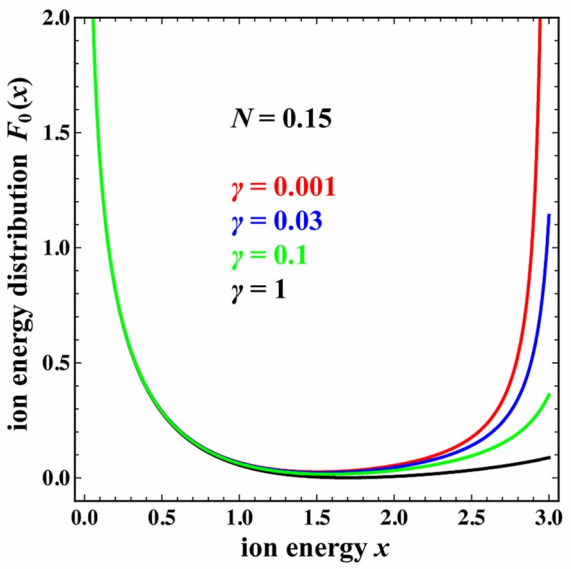

FIG. 2. (Color online) Ion energy distribution for $N=0.15$, $\beta\psi=3$, $\beta=1$, $\alpha=0$, at successive values of beam energy excess $\beta\gamma$ (namely, 0.001, 0.03, 0.1, and 1 in descending order).

The corresponding forms of the space potential $\psi-\phi(s)$ obtained from Eq. (8) are given in Fig. 3. In our example, $s(\psi)$ is close to unity but varies somewhat (logarithmically) with γ. For easier visual comparison, we have normalized every case to $s(\psi)=1$. Figure 3 shows that for small γ, a substantial extent of field-free space is created at the lower

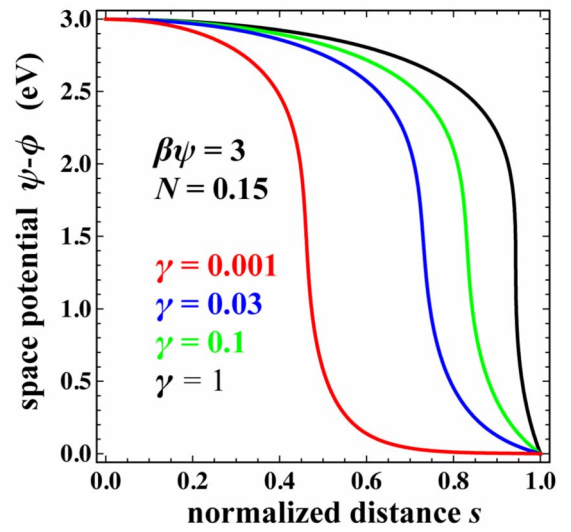

FIG. 3. (Color online) Theoretical space potential $\psi-\phi$ for $N=0.15$, $\beta\psi=3$, $\beta=1$, $\alpha=0$, at successive values of beam energy excess $\beta\gamma$ (namely, 0.001, 0.03, 0.1, and 1 from left to right).

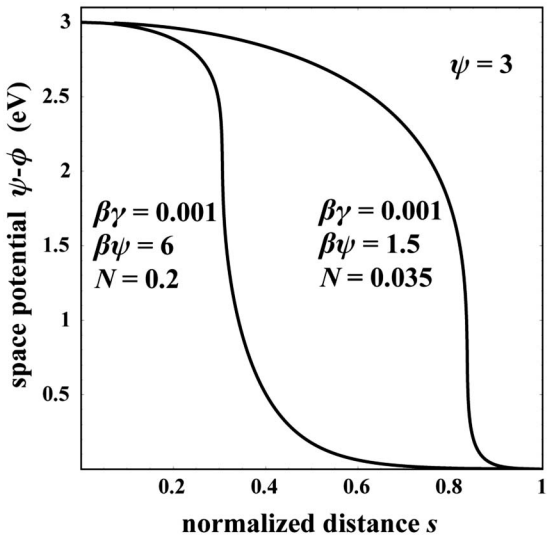

FIG. 4. Space potential $\psi-\phi$ for $\psi=3$, $\beta\gamma=0.001$, at $\beta\psi=6$ and $\beta\psi=1.5$ and $\alpha=0$. The respective values of N have been adjusted for narrowest double layers.

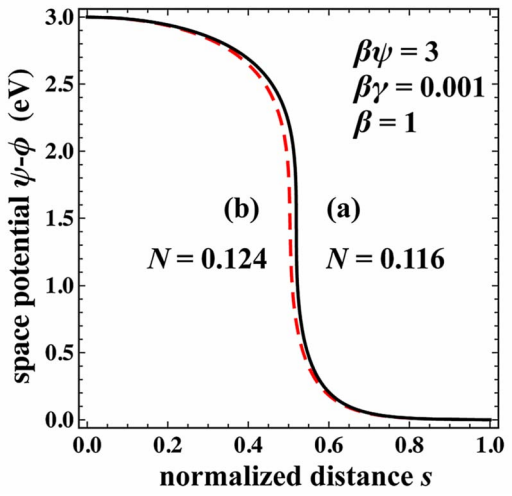

FIG. 5. (Color online) Narrowest DL solutions at $\beta\psi=3$, $\beta=1$, $\beta\gamma=0.001$, from (a) the plasma equation ($\alpha=0$, $N=0.116$, solid line) and (b) the full Poisson equation ($\alpha=2.35\times10^{-4}$, $N=0.124$, dashed line).

potential. This phenomenon is due to the steep increase of the beam density as $\phi\rightarrow\psi$, and is independent of the value of N.

The position of the sheath depends on the product $\beta\psi$. The larger this value, the closer the sheath is to the left boundary (**C** in Fig. 1, at relative potential $\psi-\phi$); in other words, for a given value of the voltage ψ (at fixed γ), decreasing the electron temperature (increasing β) displaces the sheath toward $\mathbf{g}_1$, and vice versa. Alternatively, for a given electron temperature β^{-1}, the DL can be moved closer to $\mathbf{g}_1$ by raising the intergrid potential ψ. Figure 4 shows two extreme cases ($\beta\psi=1.5$ and $\beta\psi=6$), with $\psi=3$ and $\beta\gamma=0.001$.

Decreasing N (at any γ) reduces the width of the sheath, since $F_0(x)\rightarrow0$ at the minimum. For $\psi=3$, $\gamma=0.001$, $\beta=1$, the narrowest sheath arises for $N=N_0\cong0.116$ and lies about midway between the end points (at $x\cong1.55$). This solution is shown as (a) in Fig. 5.

Of course, the mere requirement that $F_0(x)>0$ cannot fix the optimal value of N. Too narrow a sheath at a point $s=s_0$ (large $d^2\phi/ds^2$) violates the plasma approximation in the neighborhood of s_0. Moreover, at $\alpha=0$ there is no charge separation and so the narrow structure is not really a double layer. These consistency issues are remedied by imposing a nonvanishing value of α.

Proceeding by the method outlined in Sec. IV, we use the value $\alpha=2.35\times10^{-4}$, derived above, to calculate the left-hand side $\Delta n(\phi,N)=\alpha^2(d^2\phi/ds^2)=\alpha^2[dF_0(\phi)/d\phi][F_0(\phi)]^{-3}$ of Eq. (3) as a function of ϕ, corresponding to the charge-neutral ($\alpha=0$) solutions s (ϕ,N; $\psi=3$, $\gamma=0.001$, $\beta=1$). The increments $\Delta F_0(x,N)$ are then obtained by carrying out the Abel inversion of $\Delta n(\phi,N)$ numerically. For $N=0.116$, the modified ion distribution $F(x,N)=F_0(x,N)+\Delta F_0(x,N)$ is now a rapidly varying function, with closely spaced excursions below the zero axis near the point $x\cong1.55$. As before, we can increase the parameter N until $F(x,N)>0$. This yields the new critical value $N_\alpha=0.124$.

The narrowest allowed quasineutral DL solution satisfying the full Poisson equation is shown as (b) in Fig. 5, in comparison to the narrowest charge-neutral solution (a). The neutrality-breaking term $\Delta n(\phi,N_\alpha)$ is shown in Fig. 6(a). The increment $\Delta F_0(x,N_\alpha=0.124)$ is shown in Fig. 6(b). The complete distribution has now *two* closely spaced minima, as shown in Fig. 6(c). Figure 6(d) shows the Sagdeev potential $V(\phi)$ corresponding to $\phi(x,N_\alpha=0.124)$, as calculated from Eq. (5); the form of $V(\phi)$ shows immediately that the existence conditions (I)–(III) of Sec. IV are satisfied. This completes the picture drawn in Sec. IV.

The exact value of $s(\psi)$ for our solution is 1.24. This means that in order for a 1 cm discharge of Tonks-Langmuir number $\alpha=2.35\times10^{-4}$ to adapt to this solution ($\beta\psi=3$, $\beta\gamma=0.001$), at the ionization frequency $\nu=6.9\times10^4\ s^{-1}$, we need $L=0.8$ cm, $\tau=0.65$ eV, $n_0=1\times10^{13}\ \mathrm{cm}^{-3}$, and $\psi=1.95$ eV Alternatively, for $\tau=1$ eV, we should have $\nu=8.6\times10^4\ \mathrm{s}^{-1}$, $n_0=1.6\times10^{13}\ \mathrm{cm}^{-3}$, and $\psi=3$ eV.

It remains to calculate the Langmuir ratio. Using Eq. (6), with $j(\psi)=(2\pi\beta)^{-1/2}\ e^{-\beta\psi}$, and $\beta\psi=3$, $\beta\gamma=0.001$, $\beta=1$, $N=0.124$, we find $\Lambda(\psi)=159/607=0.26$. Obviously this is much too large, and therefore we are forced to adopt the view that the density n_b is due to two oppositely streaming beams of comparable energies and densities $n_{b+}\cong n_{b-}\cong n_b/2$ so that $\Lambda(\psi)\cong j(\psi)/s(\psi)=9.6/607$. Larger values of $\beta\psi$ will reduce the random flux density $j(\psi)$, and we can now readily reach $\Lambda=1/607$—in the present example, we would need $\beta\psi=4.8$.

So the model has passed the crucial test of current cancellation at $\phi=\psi$, but there is still a problem: at $\phi=0, s(\phi)\rightarrow0$, so that $\Lambda(0)\rightarrow\infty$. Including an external ion beam will remove this discrepancy, as will be seen in Sec. VII. Meanwhile, a number of idealized assumptions need to be discussed.

VI. REFINEMENTS

A. Truncated Maxwell-Boltzmann electron distribution

The assumption of Maxwell-Boltzmann electrons throughout the intergrid region is somewhat unreasonable:

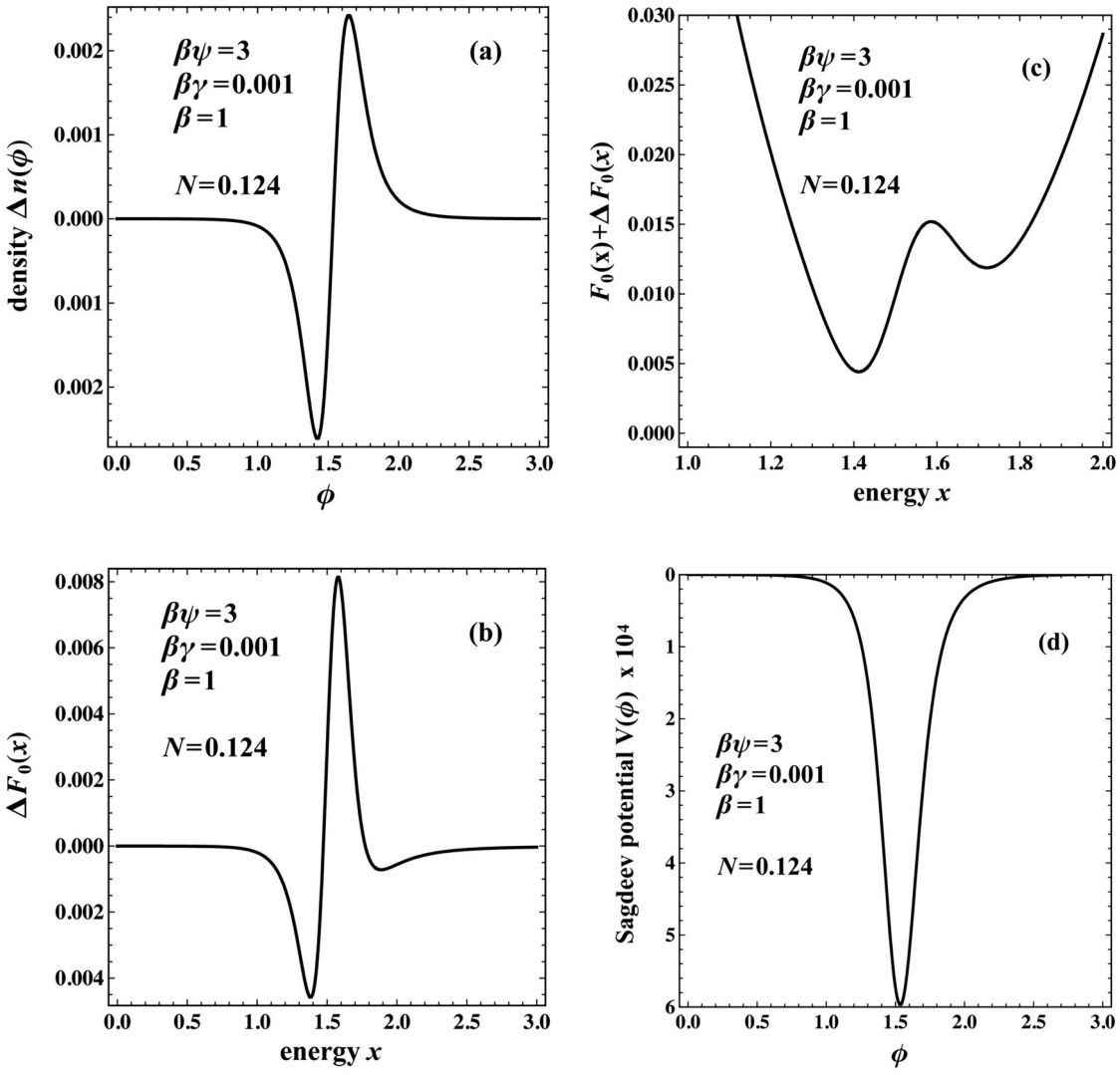

FIG. 6. Modifications due to the differential term of Eq. (2), calculated for $\beta\psi=3$, $\beta=1$, $\beta\gamma=0.001$, $\alpha=2.35\times10^{-4}$, by means of the charge-neutral ($\alpha=0$) solution $\phi(x,N)$ for $N=0.124$; (a) neutrality-breaking density increment $\Delta n(\phi)$; (b) increment $\Delta F_0(x)$; (c) complete distribution $F_\alpha(x)=F_0(x)+\Delta F_0(x)$ in the neighborhood of the minimum; (d) Sagdeev potential corresponding to $\Delta n(\phi,N=0.124)$ calculated by means of Eq. (5).

collisionless electrons with kinetic energy less than $e|\Psi|$ cannot reach the boundary. Hence the bulk electron distribution can at best only be a cutoff Maxwellian, namely, it should vanish for electron velocities V such that $mV^2/2>e(\Phi+|\Psi|)$ Integrating the Maxwellian over this bounded interval of V, converting to dimensionless variables, and normalizing to unity at $\phi=0$, yields the new form of the bulk density

$$n_{eB}(\phi)=\frac{e^{-\beta\phi}\,\mathrm{erf}\,\sqrt{\beta(\psi-\phi)}}{\mathrm{erf}\,\sqrt{\beta\psi}}. \tag{9}$$

The Abel inversion of this expression must now be carried out numerically. For modestly large $\beta\psi$, the results obtained do not differ significantly from the analytic expressions given by Eqs. (7) and (8). The main difference is that somewhat larger values of the parameter N are found for the narrowest double-layer solution. For $\psi=3$, $\beta=1$, $\gamma=0.001$, $\alpha=0$, the deepest minimum of $F_0(x)$ corresponds to $N=0.132$ (instead on 0.116) and the position of the double layer is virtually unchanged. In the optimal experimental range $4.7<\Psi<6.7$ eV, the analytic expressions (7) and (8) may be used with virtually no loss of accuracy.

B. Finite temperature beam

The effect of relaxing the assumption of a cold electron beam can be investigated by replacing the delta function distribution by the displaced Maxwellian of temperature T_b, studied by Schamel [22], namely,

$$F_b(u,\phi)=\frac{1}{\sqrt{\pi}}\exp\left\{-\frac{1}{2\rho}[(\mathrm{sgn}\,u)(u^2-2\phi)^{1/2}-u_0]^2\right\} \quad (u^2>2\phi) \tag{10}$$

in dimensionless variables, where $\rho=T_b/T$. The resulting beam density, adapted to the present definitions of ϕ, ψ, and γ, is now given by the expression

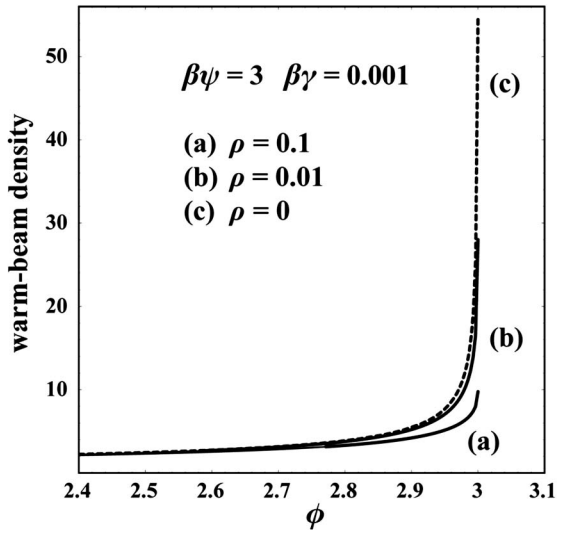

FIG. 7. Modification with temperature ratio $\rho=T_b/T$ of the electron beam density near the low-potential boundary, for $\beta\psi=3$, $\beta=1$, $\beta\gamma=0.001$.

$$n_b(\phi,\rho)=\frac{K(\phi,\gamma)+L(\phi,\gamma)}{K(0,\gamma)+L(0,\gamma)}, \tag{11}$$

in which

$$K(\phi,\gamma)=\frac{2}{\sqrt{\pi}}\int_0^{\pi/2} d\theta\sqrt{\frac{\gamma}{\rho}}\cos\theta\,\mathrm{erf}\left[\sqrt{\frac{\gamma}{\rho}}\cos\theta\right] \times\exp\left\{-\frac{1}{\rho}[\gamma\sin^2\theta+(\psi-\phi)\tan^2\theta]\right\}, \tag{12}$$

$$L(\phi,\gamma)=\exp\left[\frac{\psi-\phi-\gamma}{\rho}\right]\mathrm{erfc}\left[\sqrt{\frac{\psi-\phi}{\rho}}\right], \tag{13}$$

where in Eq. (13), $\mathrm{erfc}(y)$ is the complementary error function.

In the limit $\rho\to 0$, $L(\phi,\gamma)\to 0$ and $[K(\phi,\gamma)/K(0,\gamma)]\to[1-\phi/(\psi+\gamma)]^{-1/2}$ as it should. A comparison of this limiting value with the "warm" beam density $n_b(\phi,\rho)$ for $\rho\neq 0$ is given in Fig. 7. Increasing ρ lowers the beam density near $\phi=\psi$ and hence reduces the extent of low-potential field-free space. The effect is entirely analogous to the influence of γ shown in Fig. 3.

C. Adding a higher energy electron beam

Including an extra monoenergetic electron beam of density n_F (with $n_F/n_0=N_F$) and excess energy $\gamma_F\gg 1$ has no significant influence on the space potential. For instance, the effect on the previous example ($\alpha=0$, $\psi=3$, $\beta=1$, $N=0.116$, $\gamma=0.001$) of adding a fast beam with identical density ($N_F=0.116$), but with $\gamma_F=5$, is similar to the change caused by increasing N from N_0 to N_α, shown in Fig. 5.

VII. ADDING AN ION BEAM

The addition of an ion beam to the model is straightforward. As outlined in Sec. III, an ion beam injected into the volume of the discharge at $\Phi=0$, with initial energy $|\Theta|$ and density p_b, contributes an additional term $p_b[1-\Phi/|\Theta|]^{-1/2}$ to the ion density. Converting to dimensionless quantities, $P=p_b/n_0$, $\theta=|\Theta|/kT$, and Abel inverting this new ion term, changes Eqs. (7) and (8) to

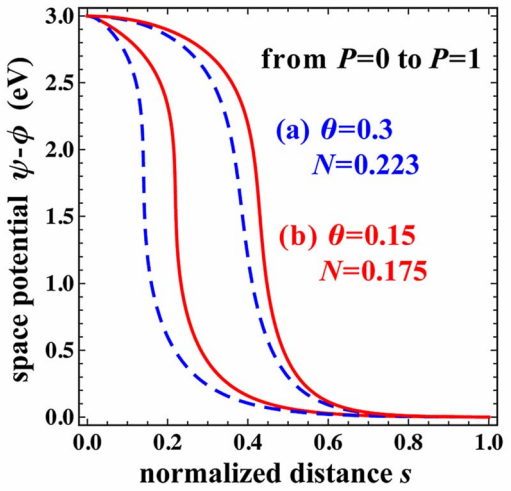

FIG. 8. (Color online) (a) (Dashed lines) Leftward displacement of a DL (parameters $\beta\psi=3$, $\beta=1$, $\beta\gamma=0.001$, $N=0.223$, $P=0$), caused by an ion beam ($P=1$, initial energy $\beta\theta=0.3$). (b) (Solid lines) Same effect on a narrower DL (parameters $\beta\psi=3$, $\beta=1$, $\beta\gamma=0.001$, $N=0.175$, $P=0$), caused by an ion beam with smaller initial energy ($P=1$, $\beta\theta=0.15$).

$$F_0(x)=\frac{\sqrt{2}}{\pi}\left\{\frac{1}{\sqrt{\beta x}}\left[1+\frac{N(\psi+\gamma)}{\psi+\gamma-x}-\frac{P\theta}{\theta+x}\right]-\sqrt{\pi}e^{-\beta x}\,\mathrm{erfi}(\sqrt{\beta x})\right\}, \tag{14}$$

$$s(\phi)=\frac{\sqrt{2}}{\pi}\left\{2N\sqrt{\beta(\psi+\gamma)}\,\mathrm{arctan}\,h\left[\frac{\sqrt{\phi}}{\sqrt{\psi+\gamma}}\right]-2P\sqrt{\beta\theta}\,\mathrm{arctan}\,h\left[\frac{\sqrt{\phi}}{\sqrt{\theta}}\right]+\sqrt{\pi}e^{-\beta\phi}\,\mathrm{erfi}(\sqrt{\beta\phi})\right\}. \tag{15}$$

To see the effect of the ion beam, we compare the example of Sec. V ($\alpha=2.35\times10^{-4}$, $\beta\psi=3$, $\beta=1$, $N=0.124$, $\beta\gamma=0.001$, $P=0$) with the new result obtained from Eqs. (14) and (15) with $P=1$, $\theta=0.3$. One difference is that $F_\alpha(x)>0$ now requires a somewhat larger value of N_α, i.e., $N_\alpha=0.223$, instead of $N_\alpha=0.124$. But the important change is that the DL moves significantly leftwards, as shown in the curves marked (a) in Fig. 8. The larger the value of P, the farther left the DL will move.

Despite these changes, the value of $s(\psi)$ is about the same as for the narrowest DL solution without the ion beam: $s(\psi)=1.34$ instead of 1.24.

It remains to evaluate the changes to the Langmuir ratio. For identical oppositely streaming electron beams at any ϕ, Eq. (6) becomes

$$\Lambda(\phi) = [j(\phi)]/[P(2\phi + 2\theta)^{1/2} + s(\psi)]. \quad (16)$$

In the current example, we find $\Lambda(\psi)=3/607$ and $\Lambda(0)=0.515$. Thus, not only has the previous unphysical divergence of $\Lambda(\phi)$ at $\phi=0$ been removed, but we are also closer to exact current cancellation at $\phi=\psi$.

At fixed P, lower values of ion initial energy θ entail smaller values of N_α and $s(\psi)$, and higher values of $\Lambda(0)$, but the DL still moves leftwards by about the same distance. Thus, for $P=1$, $\theta=0.15$, we find $N_\alpha=0.175$, $s(\psi)=1.13$, $\Lambda(\psi)=3.3/607$, $\Lambda(0)=0.73$ [see the curves marked (b) in Fig. 8].

The magnitude itself of $\Lambda(0)$ is another welcome feature, because it should allow a smooth connection to a future theory of the **K**-**C** region in Fig. 1, in which the dynamical components should dominate the stress balance, and so the Langmuir ratio at **C** would be expected to approach unity. This completes the mathematical analysis of our model.

VIII. COMPARING TO EXPERIMENT

At this stage it should be clear that the main goals set forth in Sec. II B, have been realized. In this section it will be explicitly delineated that the physical premises of the model, and the solutions described in Secs. III–VI, realistically portray every single experimental detail listed in Sec. II A.

(a) Space charge species. The basic assumption of volume ionization is verifiable visually, and the subsequent injection of an ion beam is manifest from the observed large surge in the ion current, as described in Sec. II A.

Equally plausible are the postulated negative species. Firstly, a Maxwell-Boltzmann electron component should be formed since part of the primary beam is randomized, as is always found in similar discharges (see Ref. [16]). Secondly, the display of beam components was the very purpose of the experiment in the first place: In the field-free regions of Fig. 1, as a result of inelastic collisions at thresholds E_{ex}, a cathode beam of energy E_c will show an energy spectrum with a series of maxima at all possible values of $E_c - E_{\mathrm{ex}}$. More generally, peaks occur at all values $E_c - \Sigma_i\,(c_i E^i_{\mathrm{ex}})$ by successive inelastic scattering at linear combinations $\Sigma_i\,(c_i E^i_{\mathrm{ex}})$ of important thresholds E^i_{ex}.

The maxima show up as narrow peaks in the electron energy distribution $F_e(E)$, as has been otherwise demonstrated experimentally [23] with the same mercury apparatus. Note furthermore that a truly *Maxwellian* distribution with a "bump-on-tail" has been displayed elsewhere—in a neon discharge with moving striations, as seen in Fig. 6 of Ref. [24].

(b) Beam tuning via Ψ *and the smallness of* γ. The quantity $e|\Gamma|$ in our model is given by $e|\Gamma| = E_c - \Sigma_i(c_i E^i_{\mathrm{ex}}) - e|\Psi|$. Significantly wide field-free plasma at the lower potential will be created whenever the quantities E_c, $\Sigma_i(c_i E^i_{\mathrm{ex}})$, and $e|\Psi|$ combine to produce a small enough value of $e|\Gamma|$.

Streaming beams with small $e|\Gamma|$, and similar counterstreaming beams are produced by inelastic collisions in the high- and low-potential regions, respectively. It is highly plausible therefore that, if E_c is varied at an appropriate rate, with a suitable setting of Ψ, a pair of oppositely streaming beams of small energy excess $\gamma_1 \cong \gamma_2 \ll 1$ is always present so that the theoretical mechanism causing the desired configuration of space potential can function continuously. Justifiably, this is more likely to occur when Ψ itself is in the range $4.7 < \Psi < 6.7$ spanned by the thresholds of the $6P$ states.

(c) DL position and the magnitude of Ψ. Regardless of the role of particular inelastic thresholds in establishing the lower bound $|\Psi| = \psi \cong 5$ eV, via the parameter γ, the magnitude of this bound also follows from the computed dependence of the position of the DL on the product $\beta\psi$. At any γ, wider (and presumably increasingly stable) field-free plasma at the lower potential would require that the double layer be located leftwards of the midpoint between grids. In view of the main example in Sec. V, this implies that $\beta\psi > 3$. A good setting would be $\beta\psi=6$, as shown in Fig. 4 for $\psi=3$, $\beta=2$. An electron temperature of $\tau \cong 5/6$ eV (a temperature ostensibly inherent to this mode of discharge) would then require $\psi \cong 5$ eV. Larger values of $\beta\psi$ were also found to entail larger values for the critical density fraction N due to the beam, in accordance with the observed enhancement of the low-potential peaks in the later part of the optimal range [4.7, 6.7] of settings for ψ.

(d) External ion beam. The effect of an ion beam produced externally at the ionization threshold was explained in Sec. VII. The resulting change of stress balance forces the DL further leftwards and increases the extent of low-potential plasma.

(e) Current cancellation. Also derived in Sec. VII is the virtual equality of electron and ion fluxes at the low-potential boundary, observed experimentally at the higher values of retarding potential Ψ.

(f) DL width. The width of the double layer can be estimated from the distance between maximum and minimum of the total density in Fig. 6(a), and is found to be at most 1 mm. This is entirely consistent with the magnitude of the average e^--Hg excitation free path in the pressure range 3–5 Torr of Ref. [10].

(g) Large cathode current. The condition of the large cathode current follows from the relationship between the plasma density and the length ratio α: a sufficiently narrow DL cannot develop unless α is very small. Hence n_0, the Maxwell-Boltzmann component of electron density near the virtual anode—and so also the density of the injected cathode beam—must be large enough.

Having said that, it should be noted that there is an upper limit on the strength of the cathode current. As mentioned already, the type of discharge present throughout the experiment is the "ball-of fire" mode—with the ball "anchored" at $\mathbf{g}_1$, as described in Ref. [16]. As the cathode current setting is increased, a point is reached at which this mode can no longer subsist [25]. The system cannot enter smoothly into a different mode because this transition is a potentially catastrophic event—the ball can explode.

Above a critical current, when the critical voltage $\mathbf{C}_2$ is reached, δ does not settle to an equilibrium value δ_0 but increases dramatically beyond δ_0 to a large value δ_L, the virtual anode **C** shoots upwards to $\mathbf{V}\mathbf{g}_1 + \delta_L$, and the current increases by orders of magnitude. As long as the cathode current is not too large, the system is able to react by drop-

ping the space potential: the upward path of the voltage to $\mathbf{Vg}_1+\delta_L$ at $\mathbf{C}_2$ immediately turns back (at a large value of current), the voltage of the virtual anode decreases, as does the current, until the quantity δ drops back to zero. This process then starts again and the system enters a phase of self-sustained relaxation oscillations (see Ref. [10], Sec. 8.2) described by a "hysteresis" loop in the current-voltage plane. Since the accelerating potential drops periodically below the first critical point $\mathbf{C}_1$, the tube flashes. Oscillations can last forever—and have been left on for days by the author [10]—unless the cathode current is reduced.

It is plausible from the solutions in Sec. IV that while the system is oscillating with a variable value of $\beta\psi$, the double layer is moving back and forth in the interval between the grids. Several authors have studied this phenomenon in the unstable circumstances of marginal ball-of-fire discharges (see, for instance, Ref. [26]), and have even observed period doubling routes to chaos [27]. Whether or not the apparatus of Ref. [10] can be used to measure the Feigenbaum constants as in Ref. [27] remains to be attempted.

Future work along the lines of the present model, duly adjoined to the region in Fig. 1 between the cathode **K** and the point **C**, could shed light on the critical value of α at the onset of instability, and on the role of ion starvation portrayed by the ostensible change of sign of the ion distribution near its minimum, in creating the instability, and in producing the restoring mechanism during self-sustaining oscillations.

(h) Cold cathode beam. The influence of beam temperature is explained in Sec. VI B: For a group of secondary electrons produced by inelastic scattering to acquire the character of a fairly monoenergetic beam, the primary cathode beam too must be sufficiently cold.

(i) Variable cathode beam energy. At this point, the answer to the question asked in Sec. I B is evident: The basic species of space charge necessary for creating and maintaining the space potential of Fig. 1 is not the fast primary beam of variable energy, but of its products, bulk Maxwellian electrons, slow secondary electron beams, positive ions generated throughout the volume, and an ion beam created near the exit of the electron gun. Provided that the system stays in the ball-of-fire mode of discharge in the entire range of accelerating potential, these secondary components are largely independent of the energy of the primary beam. As shown in Sec. VI C, any remaining fraction of the primary beam traversing the discharge with increasing energy can have no substantial influence on the space potential.

In actual fact, monitoring the current between the anode **A** and the cathode **K**, rather than between **A** and $\mathbf{g}_2$, can directly verify this. This arrangement eliminates the primary electron current since the anode is now below cathode potential. The resulting "excitation curve" is then the usual series of peaks superimposed on a descending (increasingly negative) background due to the ion current.

(j) Collapse of the high potential plasma. Although a small value of N is necessary for producing a free DL, larger beam densities are not detrimental to the existence of low-potential plasma. As long as the quantity γ is small, increasing N does not affect plasma conditions in the downhill region. In contrast to this, the high-potential plasma eventually collapses and the double layer reduces to a wall sheath at the fist grid ($\mathbf{g}_1$). This is easily verified by varying N in the Sagdeev potential $V(\phi,N)$: a value of N is eventually reached beyond which the tangential behavior of the inverted bell as $\phi\rightarrow 0$ disappears; the curvature changes sign and $V(\phi)$ reaches zero with a positive sign of $V''(\phi)$. In the example of Sec. IV the upper bound on N for a *free* DL is about $N=0.5$.

Note that at lower gas pressure the fraction of randomized beam is smaller and thus the value of N is necessarily larger. Therefore the high-potential spectrum should not appear at all, in accordance with the observations in Ref. [10], Sec. 8.1. Of course the experiment itself is mediocre at low pressure because the signal-to-background ratio is too low.

In conclusion, one can hardly deny that the present model is in remarkably close agreement with the mercury experiment, and should be useful for designing similar experiments with other gases and for setting objectives for future theoretical investigations.

IX. CONNECTION TO RELATED LITERATURE

The single-component Tonks-Langmuir model [14] was originally devised in order to study the plasma-sheath transition near a floating wall. For that purpose, the plasma equation is used between the center of the discharge and the "sheath edge," and the full Poisson equation between that edge and the wall. The sheath edge is identified with the point where the solution of the plasma equation becomes singular. There is vast literature on this problem going back many years, recently reviewed by Franklin [28] and Riemann [29]. In that approach, one is always faced with the subtle task of suitably joining the plasma and sheath solutions in the neighborhood of the singularity.

This difficulty does not arise in the present multicomponent model. The space charge density due to the electron beam prevents the self-consistent ion distribution from becoming negative. Therefore the singularity near the wall is smoothed out into a double layer within the volume of the discharge and the plasma equation is applicable all the way to the boundary. There is also a significant change of venue here: the wall is a conducting electrode. Hence the amplitude ψ of the "boundary layer" is not fixed by the equality of electron and ion fluxes at the boundary, but can be controlled externally.

Different kinds of multicomponent Tonks-Langmuir models have also been used to study double-layer formation. Bradley [30] has considered the sum of a Maxwellian and a "waterbag" electron distribution; other authors have used two Maxwellians of different temperature [31,32]. A common feature of these models is that—in contrast to the present case—both components of the electron density vary with ϕ in the same direction. As a result the ion energy distribution cannot rise again within the active plasma region, and the creation of a field-free region of plasma at the lower potential cannot take place.

As mentioned in the Introduction, an alternative kinetic theoretical avenue for modeling collisionless plasma double layers—extensively addressed by Schamel [33,34]—consists

in solving for the space potential using postulated distributions for *all* species of charged particles. An early attempt [35] to explain the present experiment was based on that type of approach, using truncated Maxwellian distributions for trapped particles and monoenergetic beams for free particles. Recently, the theory of Ref. [35] was refined and modified in several respects [36]. Mainly, (a) a new class of viable DL solutions was discovered and shown to obey a principle of least field energy, and (b) better quantitative agreement with the experiment of Ref. [10] was obtained by changing to the concave electron and ion distributions for trapped particles, invented by Schamel [35] for modeling electron and ion phase-space "holes." As a result, the electron beam must be slowed to almost zero velocity near the outer grid in order to produce field-free space in that area—as in the present paper, and unlike the convex case. Schamel's concave distributions are somewhat similar to the ion distributions given by Eqs. (7) and (14) above. Nevertheless, the physical basis of such distributions could not be explained realistically, and therefore the bearing of the model of Ref. [36] to the interpretation of the results of Ref. [10] was, at best, somewhat contrived.

Still, several results of that model are in good agreement with other double-layer experiments, and it is of interest that the preferred (least field energy) solutions correspond to "quasizeros"—local maxima at points ϕ_1 and ϕ_2—of the Sagdeev potential $V(\phi)$ *within* the region $0 \leqslant \phi \leqslant \psi$. Plasma conditions and the *generalized* Bohm criterion [13], given by $V''(\phi) < 0$, can thus be created dynamically *inside* a bounded discharge, regardless of nonneutrality of charge at the boundaries 0 and ψ.

Imposing *conventional* Bohm criteria (in addition to the usual boundary conditions of charge neutrality and vanishing electric field) at *the outset* prevents access to the least energy solutions of Ref. [36]; this was the view taken originally by the authors of Ref. [35]. In actual fact, Andrews and Allen [37] had already proposed the model of Ref. [35] at an earlier date, albeit with nontruncated Maxwellians, in order to model a DL experiment carried out by their group.

Lieberman and Charles [38] have recently used the Andrews-Allen theory, supplemented by a subsidiary condition based on a simplified diffusion model, in order to explain DL formation in a helicon-type discharge used in a plasma thruster for space propulsion. However, they showed that their double layer could not exist at pressures larger than 2.5 mTorr, and therefore their model is certainly not applicable to the type of discharge discussed in the present paper.

X. IS FREE-FALL MOTION JUSTIFIED?

The main shortcoming in the present theory is the glib use of free-fall motion. This is a common feature of hitherto developed kinetic DL models and is dictated primarily by mathematical convenience, since the inclusion of binary collisions would increase the difficulty by at least one order of magnitude. On the other hand, it is conceivable that double-layer formation actually occurs on the (greatly shorter?) time scale of collective events so that a collisionless approach is indeed legitimate. The very fact that the present experiment works supports this view: electrons seem to encounter tailor-made field-free drift space *before* they undergo the inelastic collisions responsible for the display of the multipeaked inelastic spectrum. In the words of the very inventor of the names "plasma" and "double sheath" [39]: "The sheath thus acts like an ideal grid for accelerating primary electrons into a field-free region."

A closely related question concerns the assumption of Maxwell-Boltzmann electrons. As pointed out by Emmert *et al.* [40], the basis of this is the experimental observation that electrons tend toward a Maxwell-Boltzmann distribution on a time scale much shorter than could be explained on a collisional basis. This is the notorious "Langmuir paradox" [41,42] most recently discussed by Tsendin [43].

For electrons, a criterion of collisionality, based on Maxwellian equilibria, has been given by Franklin (see Eq. (1.13) in Ref. [44]). Using this in the present context yields a lower limit of $n_0 = 1.5 \times 10^{12}$ cm^{-3} for free-fall motion, comfortably below the present figure of 10^{13}. Unfortunately this criterion cannot be used for ion motion because it uses the two-term approximation in Boltzmann's kinetic equation, an invalid premise for ions.

A definitive understanding of the time-scale problem in the process of formation of electrostatic phase-space structures in gas discharges is long overdue. An exciting development in this direction was reported very recently [45] and will hopefully be followed up before long.

XI. CONCLUSION

The Tonks-Langmuir model with a superposition of Maxwell-Boltzmann and monoenergetic electrons, and internally created ions, previously introduced in Ref. [15], was studied in detail. It was shown that this theory is equivalent to a Bernstein-Greene-Kruskal model, in which the scale of the postulated space potential is much larger than the Debye length, supplemented by a subsidiary condition on the potential, based on the prescribed form of the ionization mechanism [Eqs. (2) and (4)]. The model was extended to finite values of the quasineutrality parameter α and its integrity in regard to double-layer solutions was established: ideal plasma conditions on both sides of the double layer, as well as the Bohm criterion—generalized for double sheaths—are met simply by prescribing that the ion phase-space distribution should be positive.

Also discussed were the more realistic cases of a finite temperature electron beam, a bulk electron density given by a truncated Maxwell-Boltzmann distribution, and the effect of an externally prepared, and subsequently conserved, monoenergetic ion beam.

The model was inspired by, and successfully benchmarked against, experimental results obtained in a classic form of thermionic discharge, underlying a well-known and easily accessible experiment on mercury. Therefore it can be used for predicting whether a DL, of width inferior to the average excitation free path, will or will not be formed, under suitably rescaled discharge conditions, in any atomic gas,

with a carefully prepared source of primary electrons. The discharge should simply produce a sufficiently small length ratio α, and appropriate values of the density ratio N. Of course, the final answer still rests on experiment, because, as yet, whereas α can be estimated, N is only a phenomenological parameter. The *ab initio* theoretical determination of N is a tall task involving at least an approximate calculation of the electron phase-space distribution $F_e[V,\Phi(z)]$ with simplified assumptions on $\Phi(z)$, in terms of the cross sections for elastic and inelastic scattering.

ACKNOWLEDGMENT

I am greatly indebted to Robert E. Robson for many interesting discussions and for his valuable advice on the preparation of the manuscript.

[1] J. Franck and G. Hertz, Verh. Dtsch. Phys. Ges. **16**, 457 (1914).
[2] R. E. Robson, B. Li, and R. D. White, J. Phys. B **33**, 507 (2000).
[3] B. Li, R. D. White, and R. E. Robson, J. Phys. D **35**, 2914 (2002).
[4] G. Petrov and R. Winkler, J. Phys. D **30**, 53 (1997).
[5] R. E. Robson, R. D. White, and Z. Lj. Petrović, Rev. Mod. Phys. **77**, 1303 (2005).
[6] P. Nicoletopoulos and R. E. Robson, Phys. Rev. Lett. **100**, 124502 (2008).
[7] F. Sigeneger, R. Winkler, and R. E. Robson, Contrib. Plasma Phys. **43**, 178 (2003).
[8] J. Fletcher, J. Phys. D **18**, 221 (1985).
[9] P. Nicoletopoulos, in *Double Layers as Ideal Grids in Electron Spectroscopy of Atoms*, edited by M. Sanduloviciu and G. Popa, Third Symposium on Electric Double Layers, Bucharest, Romania, 1987 (Analele Stintifice ale Universitatii "Al I Cuza" din Iasi, Serie Noua Fisica), Vol. 34 (Suppl), pp. 155–160 (1988).
[10] P. Nicoletopoulos, Eur. J. Phys. **23**, 533 (2002).
[11] P. Nicoletopoulos, Eur. J. Phys. **25**, 373 (2004).
[12] R. E. Robson, P. Nicoletopoulos, B. Li, and R. D. White, Plasma Sources Sci. Technol. **17**, 024020 (2008).
[13] M. A. Raadu, Phys. Rep. **178**, 25 (1989).
[14] L. Tonks and I. Langmuir, Phys. Rev. **34**, 876 (1929).
[15] N. Jelić, M. Čerček, M. Stanojević, and T. Gyergyek, J. Phys. D **27**, 2487 (1994).
[16] E. O. Johnson, RCA Rev. **16**, 498 (1955).
[17] H. M. Jongerius, Philips Res. Rep., Suppl. **2**, 46 (1962).
[18] K.-U. Riemann, Phys. Fluids **24**, 2163 (1981).
[19] E. T. Whittaker and G. N. Watson, *A Course of Modern Analysis* (Cambridge University Press, London, 1962), p. 229.
[20] R. T. Irish and G. H. Bryant, Proc. Phys. Soc. London **84**, 975 (1964).
[21] E. R. Harrison and W. B. Thomson, Proc. Phys. Soc. London **74**, 145 (1959).
[22] H. Schamel, Phys. Scr., T **T2/1**, 228 (1982).
[23] A. D. Martin and P. J. Quinn, Am. J. Phys. **52**, 1114 (1984).
[24] S. W. Rayment and N. D. Twiddy, Br. J. Appl. Phys. **2**, 1747 (1969).
[25] L. Malter, E. O. Johnson, and W. M. Webster, RCA Rev. **12**, 415 (1951).
[26] Y. Ping *et al.*, Phys. Plasmas **8**, 5006 (2001).
[27] P. Y. Cheung and A. Y. Wong, Phys. Rev. Lett. **59**, 551 (1987).
[28] R. N. Franklin, J. Phys. D **36**, R309 (2003).
[29] K.-U. Riemann, Phys. Plasmas **13**, 063508 (2006).
[30] J. W. Bradley, J. Phys. D **34**, 3241 (2001).
[31] K. Sato and F. Miyaki, Phys. Fluids B **4**, 1247 (1992).
[32] T. E. Sheridan, N. StJ. Braithwaite, and R. W. Boswell, Phys. Plasmas **6**, 4375 (1999).
[33] H. Schamel, in *Proceedings of the First Symposium on Electric Double Layers, Roskilde, 1982*, edited by P. Michelsen and J. J. Rasmussen (Report R-472 Risø National Laboratory, Roskilde, Denmark, 1982), pp 13–39.
[34] H. Schamel, Phys. Rep. **140**, 161 (1986).
[35] H. Schamel, P. Hadjimanolaki, and P. Nicoletopoulos in *Physics and Applications of Pseudosparks*, edited by M. A. Gunderson and G. Schaefer, NATO Advanced Studies Institute, Series B: Physics (Plenum, New York, 1990), Vol. 219, pp. 277–292.
[36] P. Nicoletopoulos, e-print arXiv:physics/0410126.
[37] J. G. Andrews and J. E. Allen, Proc. R. Soc. London, Ser. A **320**, 459 (1971).
[38] M. A. Lieberman and C. Charles, Phys. Rev. Lett. **97**, 045003 (2006).
[39] I. R. Langmuir and H. A. Jones, Phys. Rev. **31**, 357 (1928).
[40] G. A. Emmert, R. M. Wieland, A. T. Mense, and J. N. Davidson, Phys. Fluids **23**, 803 (1980).
[41] I. Langmuir, Phys. Rev. **26**, 585 (1925).
[42] D. Gabor, E. A. Ash, and D. Dracott, Nature (London) **176**, 916 (1955).
[43] L. D. Tsendin, Plasma Sources Sci. Technol. **12**, S51 (2003).
[44] R. N. Franklin, *Plasma Phenomena in Gas Discharges* (Oxford University Press, Oxford, 1976).
[45] E. Wagenaars, M. D. Bowden, and G. M. W. Kroesen, Phys. Rev. Lett. **98**, 075002 (2007).